ISSN 0036-0244, Russian Journal of Physical Chemistry A, 2009, Vol. 83, No. 13, pp. 2288–2296. © Pleiades Publishing, Ltd., 2009.

PHYSICAL CHEMISTRY OF NANOCLUSTERS AND NANOMATERIALS

Investigation of Single Wall Carbon Nanotubes Electrical Properties and Normal Mode Analysis: Dielectric Effects[1]

V. S. Lee[a], P. Nimmanpipug[a], F. Mollaamin[b], N. Kungwan[a], S. Thanasanvorakun[c], and M. Monajjemi[d]

[a] *Department of Chemistry, Chiang Mai University, Chiang Mai, Thailand*

[b] *Department of Chemistry, Qom Branch, Islamic Azad University, Qom, Iran*

[c] *Department of Physics and Network for Excellence in Functional Nanomaterials, Faculty of Science, Chiang Mai University, Chiang Mai, Thailand*

[d] *Department of Chemistry, Science and Research Branch, Islamic Azad University, Tehran, Iran*

e-mail: vannajan@gmail.com

Received August 20, 2008

Abstract—Besides thermodynamic information, vibration can identify modes of a molecule by comparison of the spectroscopy and parameterize force field. By the application of group theory with the state of projection operators, a systematic method for getting the vibrational model of molecules such as the (3, 0), (4, 0), (5, 0) nanotubes was proposed. The *U* matrix from the combination of primitive's harmonic vibrations was calculated and the effect of dielectric constants on the mechanism of these vibrations in nanotubes was studied. We found that in the high dielectrics the frequency of vibration has alternative behavior, however by the decreasing of the dielectrics, this behavior change to stable situation of geometry. The calculated data shown in Tables and Figures are in correspondence with some behavior of nanotubes.

DOI: 10.1134/S0036024409130184

INTRODUCTION

Since the discovery of single-walled nanotubes (SWCNTs) by Iijima and Bethune in 1993 [1], many applications as molecular components for nanotechnology including conductivity and high-strength composites; energy storage and energy conversion devices; sensors; field emission displays and radiation sources; hydrogen storage media; and nanometer-sized semiconductor devices, probes, and interconnects are known [2–7]. Single-wall carbon nanotubes (SWCNTs) are formed by the rolling of a single layer of sp^2 carbon, called a graphene layer, into a seamless hollow cylindrical tube with nanoscale dimensions. Besides their unique physical properties (elasticity, tensile strength, stiffness, and deformation), nanotubes exhibit varying electrical properties (depending on the direction that the graphite structure spirals around the tube (quantified by the "chiral vector"), and other factors, such as doping), and can be superconductor, conductor (metallic), semiconductor or, insulator.

As this field continues to expand and grow, materials technology will produce products, components and systems that are smaller, smarter, multi-functional, environmentally compatible, more survivable, and customizable. These products will not only contribute to the growing revolutions of information and biology, but will also significantly impact manufacturing, logistics, and our culture as a whole. The development of scanning probe techniques has allowed not only the microscopy of surfaces with atomic resolution, but also the manipulation of atoms and molecules on surfaces, and many analytical techniques have been developed to allow detailed characterization of materials and structures on the atomic level with unprecedented accuracy. The utilization of materials with nanometer-sized structures will lead to innovative products which are smaller, smarter, and more multifunctional. Therefore, understanding of fundamental properties of structures at the nano scale with the aid of computational models is important to design the specific material properties.

Recently, theoretical and experimental work have predicted that the infinity length SWCNTs are π-bonded aromatic molecules that the electrical properties depending upon the tubular diameter and helical angle [8, 9]. As a graphene sheet was rolled in many ways in horizontal, vertical, and diagonal direction represent as arrow vertors, **a**, as in Fig. 1, the different types of carbon nanotubes were produced. The three main types are armchair, zig-zag, and chiral nanotube. The geometrical and electronic structure of SWCNT can be described by a chiral vector, the angle between the axis of its hexagoal pattern and the axis of the tube which is presented by the (n_1, n_2) chirality indices. When the indices are $(n_1, 0)$ called zig-zag, (n_1, n_1)

[1]The article is published in the original.

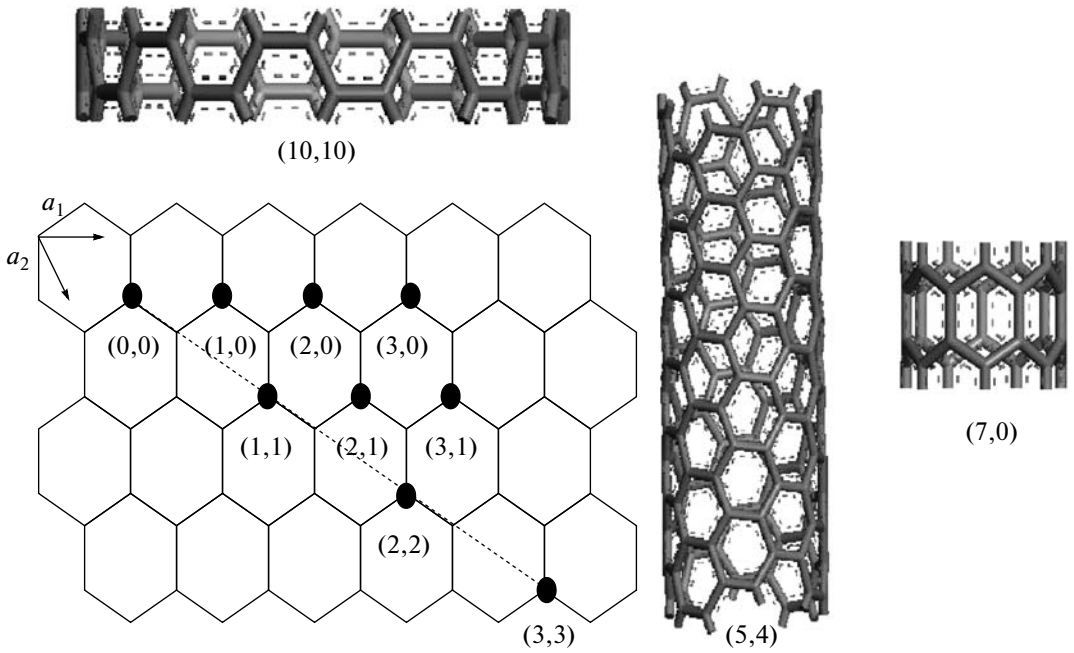

Fig. 1. The geometrical structure of SWCNT.

called armchair, and (n_1, n_2) where $n_1 \neq 0$ and $n_2 \neq 0$ known as chiral SWCNT. For $(2n_1 + n_2)/3 =$ integer, SWCNTs are metallic and others are semiconductors [10, 11]. For large diameter SWCNTs defined by $d = [3(n_1^2 + n_2^2 + n_1n_2)]^{1/2}a_{C-C}/\pi$, where a_{C-C} is the distance between neighbouring carbon atoms in the flat sheet, armchair SWCNTs are always metallic which is good for nanotechnology application. A zigzag carbon nanotube $(n_1, 0)$, is a semiconductor when $n_1/3 \neq$ integer. Such semiconductor zigzag carbon nanotubes have the ability to become base of many nanoelectronic devices and transistors.

Although, scientific efforts focused on the electrostatics properties and commercial applications of these materials [12–14], there have been no experimental structural data sufficiently accurate for the identification of the chirality indices of SWCNTs, especially for the kind of smaller diameter nanotubes. In all experimental methods for the identification commonly utilized so far is Raman spectroscopy and phonon dispersion. Phonon dispersion relations in one dimension of this system have been studied by using zonefolding along one direction of Brillouin zone considering the tube symmetry [15]. The tight binding electronic band structure and the reverse of the diameter $(1/d)$ dependence of the frequency of the radial breathing mode (RBM) were employed [16–19].

The size and chirality of the carbon nanotubes were typical determined from the SWCNT Raman energy spectra of a peak around 150–300 cm^{-1}, due to the radial breathing mode [20, 21]. Further Raman studies of SWCNT modified by various reactions e.g., oxidation reactions, ozonolysis, fluorination, residues modification [22–31] have revealed that covalent functionalization mainly affects the intensity of the Raman bands. Characterization of nanotube in adsorption gas has been studied by Monte Carlo and Langevin Dynamic Simulation [32]. It is also important to investigate the effects of diameter on a SWCNT structure how the diameter depends on geometrical parameters such as the C–C bond lengths and some of the dihedral angles of SWCNTs.

For a better understanding of the physical and electronic properties of SWCNT, a challenging task in theoretical calculation is needed to specify the material properties because of the large size of the SWCNTs and their complicated (and size-dependent) electronic structure.

A method for identifying the Raman modes of SWCNTs based on the symmetry of the vibration modes has been widely used. The Raman intensity of each vibration mode varies with polarization direction, and the relationship can be expressed as analytical functions. Each Raman-active mode of SWCNT can be distinguished from the group theory principle. The symmetry properties of periodic lattices of carbon nanotubes and the symmetry operations of chiral and achiral nanotubes [33–36] are usually described in terms of the group of the wavevector [37]. However, since nanotubes can be viewed as quasi–1D systems, the line groups approach by Damnjanovic et al. [33] is suited to describe nanotube properties.

NANOTUBE STRUCTURE AND GROUP THEORY

As described earlier, the properties of nanotubes are determined by their diameter and chiral angle, both of which depend on n_1 and n_2. Typically, SWCNT is presented by a pair of integers (n_1, n_2). Its geometrical structure as shown in diagram can be represented in term of a chiral vector **C** on a two-dimensional sp^2-carbon sheet where $\mathbf{C} = n_1\mathbf{a}_1 + n_2\mathbf{a}_2$ with integer n_1 and n_2. Here, $\mathbf{a}_1$ and $\mathbf{a}_2$ represent the unit vectors of the hexagonal graphene lattice. This sheet is then rolled up to a cylinder so that **C** becomes the circumference of the tube. The direction of the nanotube axis is naturally perpendicular to **C**. The diameter, d, is simply the length of the chiral vector divided by 1/4, and $d = (3/\pi)^{1/2}a_{C-C}(n_1^2 + n_2^2 + n_1n_2)^{1/2}$, where a_{C-C} is the distance between neighbouring carbon atoms in the flat sheet. In turn, the chiral angle (θ) is given by $\tan^{-1}(3n/(2n_2 + n_1))^{1/2}$.

The translational period, a, is the shortest possible lattice vector along z direction. The translatory unit cell of a nanotube is a cylinder with a length in tube axis direction equal to the magnitude of the translation vector **T** as shown in Fig. 1 which can be calculated as following equation:

$$a = -\frac{2n_2 + n_1}{nR}a_1 + \frac{2n_1 + n_2}{nR}a_2$$

with

$$a = |a| = \frac{3(n_1^2 + n_2^2 + n_1n_2)^{1/2}}{nR}a_0,$$

where n is the greatest common divisor of n_1 and n_2,

$$\text{if } (n_1 - n_2)/3n \neq \text{integer, then } R = 1,$$

$$\text{if } (n_1 - n_2)/3n = \text{integer, then } R = 3,$$

and $\mathbf{a}_1$ and $\mathbf{a}_2$ form an angle of 60° and their length is $|a_1| = |a_2| = a_0 = 2.461$ Å.

Since the translational period, a, depends inversely on n and R the translation periodicity and thus the number of carbon atoms varies strongly for tubes with similar diameter. The number of graphene cells in the nanotube unit cell (n_C) obtained from:

$$n_C = 2q = 4(n_1^2 + n_2^2 + n_1n_2)/nR.$$

The groups of infinite line L are products $L = ZP$, where P is a point group and Z is the group of translations (screw axis, pure translations, and glide planes). Applying the above symmetry formulation to armchair $(n_1 = n_2)$ and zig-zag $(n_2 = 0)$ nanotubes, such nanotubes with no caps have a isogonal point groups given by q (the number of graphene cells in the unit cell of the nanotubes) namely, D_{nd} when n is odd, D_{nh} when n is even, or $D_{qh} = D_{2nh}$ for achiral and D_q for chiral tubes. Whether the symmetry groups for armchair and zigzag tubules are taken to be D_{nd} or D_{nh}, the calculated vibrational frequencies will be the same; the symmetry assignments for these modes, however, will be different. It is, thus, expected that modes that are Raman or IR-active under D_{nd} (or D_{nh}) but are optically under D_{2nh} will only show a weak activity resulting from the fact that the existence of caps lowers the symmetry that would exist for a nanotube of infinite length.

ACTIVE MODES OF RAMAN AND INFRARED SPECTROSCOPY

The phonon symmetries are found by decomposing the dynamical representation into its irreducible representations using symmetries of carbon and other nanotubes studied for line groups [38]. One direct set up of the dynamical representation from the atomic and vector representation is to use factor group analysis. A representation can be decomposed into the sum of its irreducible representations by the following formula

$$f_\alpha = \frac{1}{g}\sum_G \chi^{(\alpha)}(G)^*\chi^{(\Gamma_{DG})}(G),$$

where f_α is the appearance frequency of the irreducible representation α, g is the order of the symmetry group; the sum is over all symmetry operations G.

The Raman Γ_R and infrared active Γ_{IR} vibrations transform according to the representation of the second rank tensor and the vector representation, respectively [39].

$$\Gamma_R = [\Gamma_{vec} \otimes \Gamma_{vec}]$$
$$= A_{1g} \oplus E_{1g} \oplus E_{2g}(\oplus A_{2g}),$$
$$\Gamma_{IR} = \Gamma_{vec} = A_{2u} \oplus E_{1u}.$$

According to the symmetries of Raman-active modes [40] for the armchair carbon nanotube with the chair vector (n_1, n_2), the point group for this kind nanotube belongs to D_{nh} when n is even and its Raman-active modes are denoted by $A_{1g} + E_{1g} + E_{2g}$. Three flavors of modes are longitudinal, transversal radial (orthogonal to tube surface) and transversal axial (parallel to tube surface). Satio et al. [41] pointed out that the low frequency A_{1g} mode is a radial breathing mode and two high frequency is belong to E_g modes, E_{1g} and E_{2g}; E mode has the same displacement pattern with additional standing wave on the circumference.

COMPUTATIONAL DETAILS

The zig-zag single-walled carbon nanotubes (SWCNTs) with (3, 0), (4, 0), and (5, 0) structure were built using the tool in HyperChem7.0 [42]. The symmetries of the nanotube are D_{3d}, D_{4d}, and D_{5d} respectively. Four different systems were studied in this work as follow: (1) gas-phase SWCNT, (2) SWCNT with 23

water molecules in the $a \times b \times c$ box, (3) SWCNT with 23 methanol molecules in the $a \times b \times c$ box, and (4) SWCNT with mixed solvent of water and methanol molecules in the $a \times b \times c$ box. Energy minima of systems (2)–(4) were carried out by Metropolis Monte-Carlo (MC) calculation which generate random configurations in regions of space that make the important contributions to the calculation of thermodynamic averages. Then the ab initio and semiemperical with AM1 were used to optimize the structure of the nanotubes. All the normal mode frequencies and IR intensity were calculated using the optimized structures.

PROJECTION OPERATORS

To find a function or the displacement pattern of eigenvectors transforming as a particular irreducible representation, the projection operators in group theory have been applied. Consider an arbitrary function F. This function can, in general, be expanded into several irreducible representations $F = \sum_\alpha \sum_n c_\alpha^n \zeta_\alpha^n$ where α labels the irreducible representations, c_α^n are the coefficients of the expansion, and the ζ_α^n are functions transforming according to the representation α. A projection operator defined by

$$P_{l(n)}^{(\beta)} = \frac{d_\beta}{g} \sum_G D_{\ln}^{(\beta)}(G)^*(G),$$

applied to F picks out the symmetry adapted function $\zeta_l^{(\beta)}$. In this equation d_β is the degeneracy of the irreducible representation β, g the order of the symmetry group, G are the symmetry operations, and $D_{ln}^{(\beta)}$ is the lnth element of the representation matrix $D^{(\beta)}$. From a given function, and its irreducible presentation, functions can be generating if that function has a "component" or a "non-zero projection" along the irreducible presentation of interest. This explains the name of "projector." As an example, if there is an orthonormal set Li of the function φ_1^i, φ_2^i, ..., φ_{Li}^i which is used to form the ith irreducible representation of a group by order h, for each operator, $\mathbf{R}$, in the group, by definition we can have:

$$\mathbf{R}\varphi_t^i = \Sigma_s \varphi_s^i \Gamma(R)_{st}^i. \quad (1)$$

If we multiply (1) by $[\Gamma(R)_{s't'}^i]^*$ and sum all over the symmetrical functions in the group we will have:

$$\Sigma_R [\Gamma(R)_{s't'}^i]^* \mathbf{R}\varphi_t^i = \Sigma_R \Sigma_s \Gamma \varphi_s^i \Gamma(R)_{st}^i \Gamma(R)_{s't'}^i]^*. \quad (2)$$

Considering φ_s^i are functions independent from R, the right side of (2) can be written as:

$$\Sigma_s \varphi_s^i \Sigma_R \Gamma(R)_{st}^i [\Gamma(R)_{s't'}^i]^*.$$

So we have a series of Li terms and each of them are equal to a production of φ_s^i and a coefficient. These coefficients are following the orthogonality rule:

$$\Sigma_R \Gamma(R)_{st}^i [\Gamma(R)_{s't'}^i]^* = h/(L_i L_j)^{1/2} \delta_{ij} \delta_{ss'} \delta_{tt'}. \quad (3)$$

By use of the Eq. (3), the Eq. (2) is simplified as follows:

$$\Sigma_R [\Gamma(R)_{s't'}^i]^* \mathbf{R}\varphi_t^i = (h/L_j)\varphi_{s'}^i \delta_{ij} \delta_{tt'}. \quad (4)$$

Now, by introducing

$$\mathbf{P}_{s't'}^j = L_j/h \Sigma_R \Gamma(R)_{st}^i [\Gamma(R)_{s't'}^i]^* \mathbf{R}. \quad (5)$$

The Eq. (4) gives the following form:

$$\mathbf{P}_{s't'}^j \varphi_t^i = \varphi_{s'}^i \delta_{ij} \delta_{tt'}. \quad (6)$$

The $\mathbf{P}_{s't'}^j$ is call projection operator. The application of this operator on each φ_t^i is non-zero only when this function or some of its terms is a function of $\varphi_{s'}^i$. One of the most important application of this operator is projecting function φ_t^i from any function φ_t^i. In other words

$$\mathbf{P}_{t''t}^j \varphi_t^i = \varphi_{t'}^i \delta_{ij} \delta_{tt'}. \quad (7)$$

By use of the projection operator on the base of L_j diagonal elements of a matrix, we can have some φ_t^i functions, which are the bases for the jth irreducible presentation [43].

THE RELATION BETWEEN PROJECTION AND TRANSFER OPERATORS

Assume that $\Gamma_k(p)_{ij}$ is the ijth element of the matrix which shows the pth operator ($\mathbf{O}p$) in the kth irreducible presentation. By this assumption the operator $\mathbf{O}_{k,ij}$ is defined as follows

$$\mathbf{O}_{k,ij} = L_k/h \Sigma_p \Gamma_k(p)_{ij}^* \mathbf{O}p, \quad (8)$$

where h is group order and L_k is the presentation dimension. If $i = j$ these operators called. Projection operators, $\mathbf{P}_{k,ii}$, in other words:

$$\mathbf{P}_{k,ij} = \mathbf{O}_{k,ii}. \quad (9)$$

The non-diagonalized operators are called Transfer operators or shift operators,

$$\mathbf{T}_{k,ij} = \mathbf{O}_{k,ij}, \quad i \neq j. \quad (10)$$

In one-dimensional presentations $\mathbf{P}_{k,ij}$ and $\mathbf{O}_{k,ii}$ are the same and we have no $\mathbf{T}_{k,ij}$. With use of the above definitions, making the irreducible basis becomes possible in the following way.

At first the point group of the molecule is determined. Then the character of the system (Γ_{angles} or

The combination and their normalization coefficients of (3, 0) nanotube in D_{3d} point group

C_{2v}	E	C_2	σ_v	σ'_v	Irreduced presentation	Primitives	Linear combination of primitives based on their symmetric A_1, A_2, B_1, B_2
Γ_1	3	1	1	3	$2A_1$ B_2	3	$S_1(A_1) = \frac{1}{\sqrt{2}}(R_1 + R_2)$, $S_2(B_2) = \frac{1}{\sqrt{2}}(R_1 - R_2)$, $S_3(A_1) = R_{31}$
Γ_2	3	1	1	3	$2A_1$ B_2	3	$S_4(A_1) = \frac{1}{\sqrt{2}}(R_8 + R_9)$, $S_5(B_2) = \frac{1}{\sqrt{2}}(R_8 - R_9)$, $S_6(A_1) = R_{51}$
Γ_3	3	1	1	3	$2A_1$ B_2	3	$S_7(A_1) = \frac{1}{\sqrt{2}}(R_{14} + R_{15})$, $S_8(B_2) = \frac{1}{\sqrt{2}}(R_{14} - R_{15})$, $S_9(A_1) = R_{43}$
Γ_4	3	1	1	3	$2A_1$ B_2	3	$S_{10}(A_1) = \frac{1}{\sqrt{2}}(R_{20} + R_{22})$, $S_{11}(B_2) = \frac{1}{\sqrt{2}}(R_{20} - R_{22})$, $S_{12}(A_1) = R_{52}$
Γ_5	3	1	1	3	$2A_1$ B_2	3	$S_{13}(A_1) = \frac{1}{\sqrt{2}}(R_{25} + R_{26})$, $S_{14}(B_2) = \frac{1}{\sqrt{2}}(R_{25} - R_{26})$, $S_{15}(A_1) = R_{57}$
Γ_6	3	1	1	3	$2A_1$ B_2	3	$S_{16}(A_1) = \frac{1}{\sqrt{2}}(R_{29} + R_{30})$, $S_{17}(B_2) = \frac{1}{\sqrt{2}}(R_{29} - R_{30})$, $S_{18}(A_1) = R_{64}$
Γ_7	14	2	2	2	$5A_1$ $3A_2$ $3B_1$ $3B_2$	14	$S_{19}(A_1) = \frac{1}{2}(R_5 + R_{17} + R_3 + R_2)$, $S_{20}(A_2) = \frac{1}{2}(R_5 + R_3 - R_{17} - R_2)$, $S^*_{20}(A_2) = \frac{1}{2}(R_{17} + R_2 - R_5 - R_3)$, $S_{21}(A_2) = \frac{1}{2}(R_3 - R_5 + R_2 - R_{17})$, $S_{22}(A_1) = \frac{1}{\sqrt{2}}(R_4 + R_{16})$, $S_{23}(A_1) = \frac{1}{\sqrt{2}}(R_4 - R_{16})$, $S_{24}(A_1) = \frac{1}{\sqrt{2}}(R_{40} + R_{52})$, $S_{25}(B_2) = \frac{1}{\sqrt{2}}(R_{40} - R_{52})$, $S_{26}(A_1) = \frac{1}{\sqrt{2}}(R_{51} + R_{50})$, $S_{27}(B_2) = \frac{1}{\sqrt{2}}(R_{51} - R_{50})$, $S_{28}(A_1) = \frac{1}{2}(R_{29} + R_{30} + R_{51} + R_{37})$, $S_{29}(B_1) = \frac{1}{2}(R_{29} - R_{50} + R_{53} - R_{37})$, $S^*_{29}(B_1) = \frac{1}{2}(R_{30} + R_{50} - R_{29} - R_{53})$, $S_{30}(A_2) = \frac{1}{2}(R_{29} + R_{37} - R_{53} - R_{30})$
Γ_8	14	2	2	2	$5A_1$ $3A_2$ $3B_1$ $3B_2$	14	$S_{31}(A_1) = \frac{1}{2}(R_{11} + R_6 + R_7 + R_9)$, $S_{32}(A_2) = \frac{1}{2}(R_{11} + R_7 - R_6 - R_9)$, $S^*_{32}(A_2) = \frac{1}{2}(R_6 + R_9 - R_{11} - R_7)$, $S_{33}(B_1) = \frac{1}{2}(R_7 - R_{11} + R_9 - R_6)$, $S_{34}(A_1) = \frac{1}{\sqrt{2}}(R_4 + R_{10})$, $S_{35}(B_2) = \frac{1}{\sqrt{2}}(R_4 - R_{10})$, $S_{36}(A_1) = \frac{1}{\sqrt{2}}(R_{43} + R_{54})$, $S_{27}(B_2) = \frac{1}{\sqrt{2}}(R_{43} - R_{54})$, $S_{38}(A_1) = \frac{1}{\sqrt{2}}(R_{55} + R_{56})$, $S_{39}(B_2) = \frac{1}{\sqrt{2}}(R_{55} - R_{56})$, $S_{40}(A_1) = \frac{1}{2}(R_{33} + R_{34} + R_{57} + R_{31})$, $S_{41}(B_1) = \frac{1}{2}(R_{33} - R_{31} + R_{57} - R_{34})$, $S^*_{41}(B_1) = \frac{1}{2}(R_{31} + R_{34} - R_{33} - R_{57})$, $S_{42}(A_2) = \frac{1}{2}(R_{33} + R_{31} - R_{57} - R_{34})$

Table. (Contd.)

C_{2v}	E	C_2	σ_v	σ'_v	Irreduced presentation	Primitives	Linear combination of primitives based on their symmetric A_1, A_2, B_1, B_2
Γ_9	14	2	2	2	$5A_1$ $3A_2$ $3B_1$ $3B_2$	14	$S_{43}(A_1) = \frac{1}{2}(R_{21} + R_{16} + R_{18} + R_{17})$, $S_{44}(A_2) = \frac{1}{2}(R_{21} - R_{26} + R_{17} - R_{18})$, $S^*_{44}(A_2) = \frac{1}{2}(R_{26} + R_{17} - R_{21} - R_{18})$, $S_{45}(B_1) = \frac{1}{2}(R_{18} - R_{21} + R_{17} - R_{26})$, $S_{46}(A_1) = \frac{1}{\sqrt{2}}(R_{19} + R_{25})$, $S_{47}(B_2) = \frac{1}{\sqrt{2}}(R_{19} - R_{25})$, $S_{48}(A_1) = \frac{1}{\sqrt{2}}(R_{48} + R_{51})$, $S_{49}(B_2) = \frac{1}{\sqrt{2}}(R_{48} - R_{51})$, $S_{50}(A_1) = \frac{1}{\sqrt{2}}(R_{58} + R_{59})$, $S_{51}(B_2) = \frac{1}{\sqrt{2}}(R_{58} - R_{59})$, $S_{52}(A_1) = \frac{1}{2}(R_{60} + R_{41} + R_{45} + R_{47})$, $S_{53}(B_1) = \frac{1}{2}(R_{60} - R_{41} + R_{45} - R_{47})$, $S^*_{53}(B_1) = \frac{1}{2}(R_{41} + R_{47} - R_{60} - R_{45})$, $S_{54}(A_2) = \frac{1}{2}(R_{60} - R_{41} - R_{45} + R_{47})$
Γ_{10}	14	2	2	2	$5A_1$ $3A_2$ $3B_1$ $3B_2$	14	$S_{55}(A_1) = \frac{1}{2}(R_{13} + R_{15} + R_{18} + R_{12})$, $S_{56}(A_2) = \frac{1}{2}(R_{13} - R_{15} + R_{18} - R_{12})$, $S^*_{56}(A_2) = \frac{1}{2}(R_{15} + R_{12} - R_{13} - R_{18})$, $S_{57}(B_1) = \frac{1}{2}(R_{18} - R_{13} + R_{12} - R_{15})$, $S_{58}(A_1) = \frac{1}{\sqrt{2}}(R_{10} + R_{16})$, $S_{59}(B_2) = \frac{1}{\sqrt{2}}(R_{10} - R_{16})$, $S_{60}(A_1) = \frac{1}{\sqrt{2}}(R_{61} + R_{46})$, $S_{61}(B_2) = \frac{1}{\sqrt{2}}(R_{61} - R_{46})$, $S_{62}(A_1) = \frac{1}{\sqrt{2}}(R_{62} + R_{63})$, $S_{63}(B_2) = \frac{1}{\sqrt{2}}(R_{62} - R_{63})$, $S_{64}(A_1) = \frac{1}{2}(R_{35} + R_{64} + R_{39} + R_{65})$, $S_{65}(B_1) = \frac{1}{2}(R_{35} - R_{65} + R_{39} - R_{64})$, $S^*_{65}(B_1) = \frac{1}{2}(R_{64} + R_{65} - R_{35} - R_{39})$, $S_{66}(A_2) = \frac{1}{2}(R_{41} + R_{14} - R_{47} - R_{13})$

Γ_{bonding}) is calculated. By use of the standard reduce formulation these characters can be reduced to give the irreducible presentations:

$$n_\Gamma = \frac{1}{h}\Sigma_g n_g \chi_R \chi_\Gamma, \quad (11)$$

where h is the order of the group, n_g is the number of the symmetry operation in the class of g, χ_R is the character of reducible presentation and χ_Γ is the character of irreducible presentation for the symmetric operations of class g. In this part there is a note about the reducing the $C_{\infty v}$ and $D_{\infty h}$ point groups. The method of reduce is a different from the normal method of reduce. For more information see [44–50].

At the next step, the interested function is written by use of the projection operator. A set of the results gives the internal coordinate system for a given point group. There are several examples to illustrate this procedure in table. With use of the resulting coordinate system, the U Matrix (UMAT) can be written easily. These are matrices which perform the linear transformations on the internal coordinates sets [51].

RESULTS AND DISCUSSION

Linear Combination of Primitive's Harmonic Vibrations and UMAT

The molecules and their internal coordinates of D_{4d} have been given in Fig. 2. By following the above steps a complete set of the linear combinations and their normalization coefficients are achieved. The irreducible representations of the symmetry group are given by A and B. These data are given in table. We use the application of projection operator method in finding the coordinate system, and by using it the U matrix is written and finally the frequencies and distributions of peak position are achieved. The (3, 0), (4, 0), (5, 0) zig-zag nanotubes were investigated. They have 66, 138, and 174 normal modes, respectively. The character of the system assigned by Γ was calculated from the character tables. Vibrational Calculation was carried out by the MOLVIB algorithms and by Hyper Chem. Calculation and a few sets of calculation were performed. Molecular motions can be assigned by the potential energy distribution (PED) analysis among internal coordinates by the method of the projection

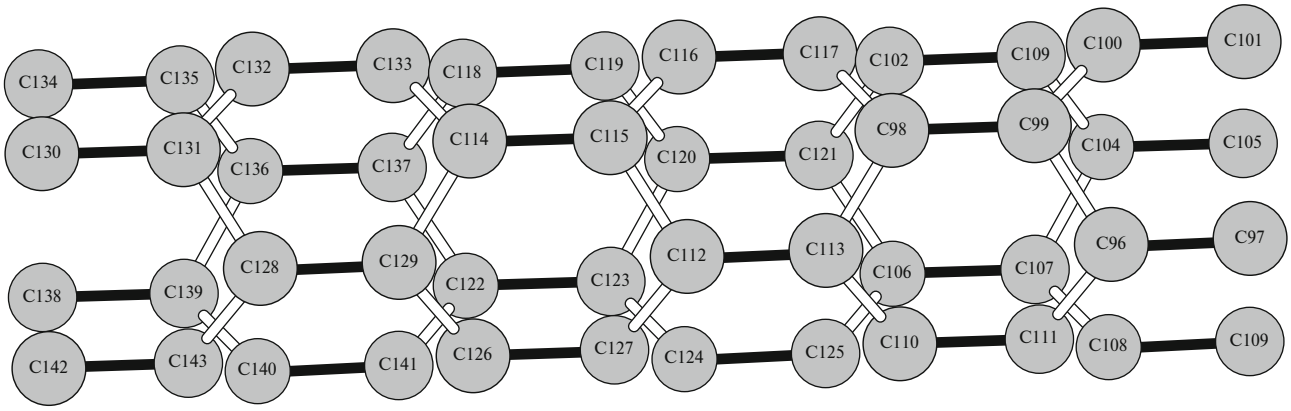

Fig. 2. The structure of (4, 0) nanotube in D_{4d} point group.

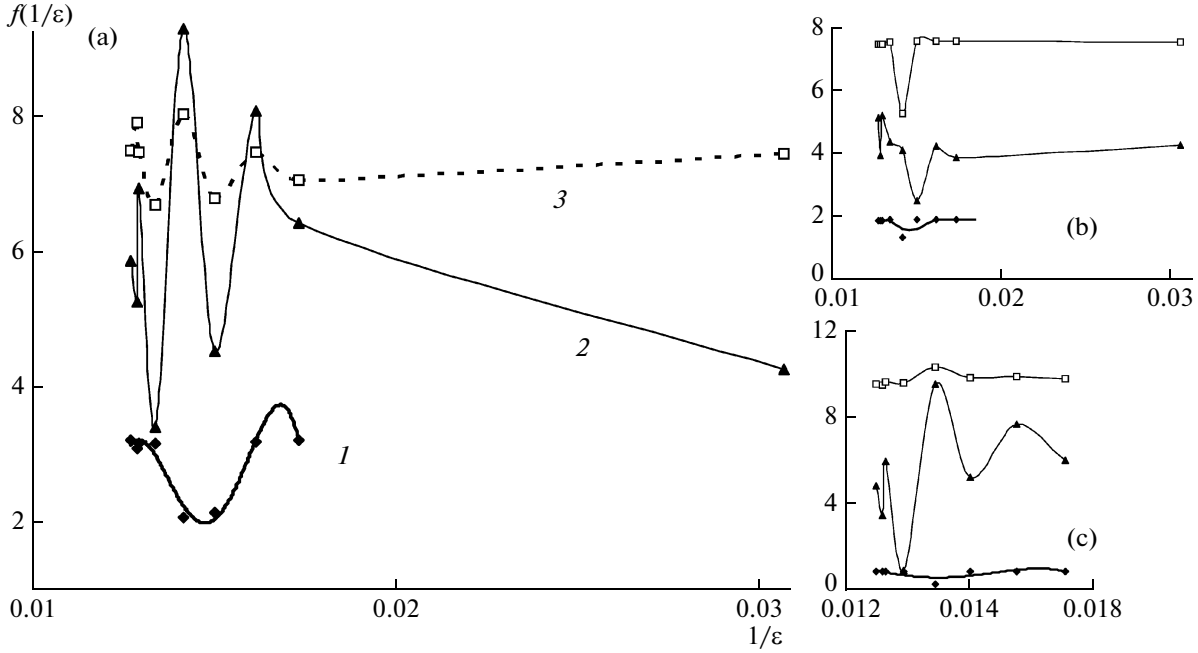

Fig. 3. The natural logarithms of the potential energy (*1*), intensity (*2*), and frequency (*3*) of three normal modes (a) 1, (b) 61, (c) 66 versus inverse of dielectric constant for nanotube (3, 0) with D_{3d} point group by AM1 calculation.

operator. There are good agreements between the most cases.

Normal Mode Dependence on Dielectric

As can be inferred from the Figs. 3–5, there are good agreements between the semi and Monte-Carlo and even ab initio calculation. From Fig. 3 we have two maximum for both of energy and frequency in the dielectric between 77.40 up to 70.42 and also the third maximum is located in the 61.76. This region range is considered to be the unstable geometry of nanotubes which are very sensitive to dielectric. After these range the frequency, intensity and energy goes toward a stable geometry which are not sensitive to dielectric. The same results are obtained in the Figs. 1b, 1c for D_{3d} of normal mode 61 and 66 respectively. In the Fig. 4a–4c, similar to normal mode 1 and 131 and 138 are shown respectively for nanotube (4, 0) in D_{4d} point group, a common general behavior is observed in this nanotube as same as (3, 0) nanotube, only with a shift in data, this shift is due to the difference between the geometrical structures of two nanotubes.

Potential Energy Dependence on the Dielectrics of Zig-zag Nanotubes

In Fig. 5 three line of potential energy for three nanotubes are shown by the Monte-Carlo calculation versus dielectric constants. For D_{3d} symmetric nano-

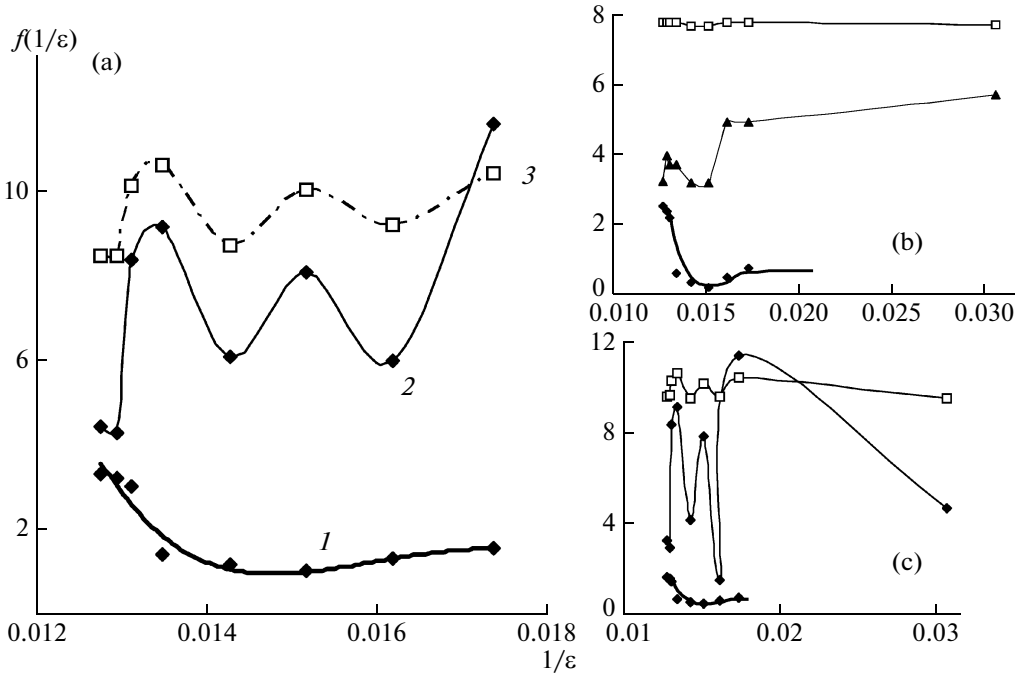

Fig. 4. The logarithms of the potential energy (*1*), intensity (*2*), and frequency (*3*) of three normal modes (a) 1, (b) 131, (c) 138 versus inverse of dielectric constant for nanotube (4, 0) with D_{4d} point group by AM1 calculation.

tube, the logarithm of potential energy increases as the dielectric constant reduces from 78.39 up to 76.10 while the D_{4d} and D_{5d} symmetries show an unchanged potential energy in this region. Beyond this point, the potential energy of D_{4d} and D_{5d} nanotubes drop and rise again to be in a new equilibrium, whereas the potential energy of the D_{3d} mostly constant as the dielectric constant decreases. There are some changing in the energy in variable with the dielectrics above 60, and by decreasing the dielectrics the energy of three nanotubes goes toward constant variables. Similar trends between three figures and there are very good agreement with ab initio calculation.

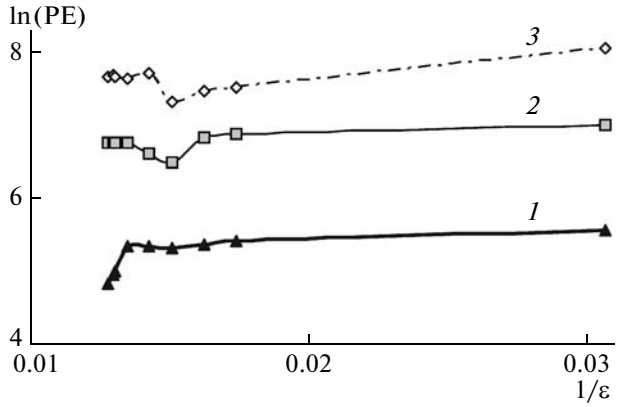

Fig. 5. The logarithms of the potential energy (PE) of three different zigzag nanotubes (*1*) D_{3d}, (*2*) D_{4d}, (*3*) D_{5d} versus inverse of dielectric constant by MC simulations.

CONCLUSIONS

The geometry and electrical properties of nanotube are very sensitive to dielectric constants. The normal modes also will be changed in the high dielectric constants. With the calculation of the normal modes using the *U* Matrix it is possible to get the *F* Matrix from the multiplication of frequency to the *U* Matrix. Solving the determination of *F* Matrix versus dielectric can be useful for understanding of the electrical behavior of nanotubes in the quantitative structure activity relationship (QSAR) studies.

REFERENCES

1. D. S. Bethune, C. H. Kiang, M. S. deVries, et al., Nature **363**, 605 (1993).
2. P. M. Ajayan, O. Stephan, C. Colliex, and D. Trauth, Science **265**, 1212 (1994).
3. Y. Saito, K. Hamaguchi, K. Hata, et al., Nature **389**, 554 (1997).
4. W. A. de Heer, A. Chatelain, and D. Ugarte, Science **270**, 1179 (1995).
5. P. G. Collins, A. Zettl, H. Bando, et al., Science **278**, 100 (1997).
6. M. B. Nardelli, B. I. Yakobson, and J. Bernholc, Phys. Rev. B **57**, R4277 (1998).
7. J. Y. Huang, S. Chen, Z. F. Ren, et al., Nanolett. **6**, 1699 (2006).
8. Z. Y. Zhou, M. Steigerwald, M. Hybertsen, et al., J. Am. Chem. Soc. **126**, 3597 (2004).

9. V. Barone, J. E. Peralta, M. Wert, et al., Nanolett. **5**, 1621 (2005).
10. R. Saito, G. Dresselhaus, and M. S. Dresselhaus, Chem. Phys. Lett. **195**, 537 (1992).
11. R. Saito, M. Fujita, G. Dresselhaus, and M. S. Dresselhaus, Phys. Rev. B **46**, 1804 (1991).
12. M. Ouyang, J. L. Huang, and C. M. Lieber, Acc. Chem. Res. **35**, 1018 (2002).
13. C. L. Kane and E. J. Mele, Phys. Rev. Lett. **78**, 1932 (1997).
14. A. Hartschuh, H. N. Pedrosa, J. Peterson, et al., Chem. Phys. Chem. **6**, 577 (2005).
15. P. C. Eklund, J. M. Holden, and R. A. Jishi, Carbon **33**, 959 (1995).
16. A. Jorio, R. Saito, J. H. Hafner, et al., Phys. Rev. Lett. **86**, 1118 (2001).
17. S. M. Bachilo, M. S. Strano, C. Kittrell, et al., Science **298**, 2361 (2002).
18. R. Pfeier, H. Kuzmany, Ch. Kramberger, et al., Phys. Rev. Lett. **90**, 225501 (2003).
19. J. Kurti, V. Solyomi, M. Kertesz, et al., Carbon **42**, 971 (2004).
20. J. Maultzsch, H. Telg, S. Reich, and C. Thomsen, Phys. Rev. B **72**, 205438 (2005).
21. A. Jorio, C. Fantini, M. Pimenta, et al., Phys. Rev. B **71**, 075401 (2005).
22. M. S. Strano, C. A. Dyke, M. L. Usrey, et al., Science **301**, 1519 (2003).
23. P. Umek, J. W. Seo, K. Hernadi, et al., Chem. Mater. **15**, 4751 (2003).
24. H. Q. Peng, L. B. Alemany, J. L. Margrave, and V. N. Khabashesku, J. Am. Chem. Soc. **125**, 15174 (2003).
25. J. L. Bahr, J. P. Yang, D. V. Kosynkin, et al., J. Am. Chem. Soc. **123**, 6536 (2001).
26. M. Holzinger, J. Abraha, P. Whelan, et al., J. Am. Chem. Soc. **125**, 8566 (2003).
27. E. T. Mickelson, C. B. Huffman, A. G. Rinzler, et al., Chem. Phys. Lett. **296**, 188 (1998).
28. L. T. Cai, J. L. Bahr, Y. X. Yao, and J. M. Tour, Chem. Mater. **14**, 4235 (2002).
29. S. Banerjee and S. S. Wong, J. Phys. Chem. B **106**, 12144 (2002).
30. J. E. Herrera and D. E. Resasco, Chem. Phys. Lett. **376**, 302 (2003).
31. M. T. Martinez et al., Nanotechnology **14**, 691 (2003).
32. M. Monajjemi and L. Mahdavian, Bull. Chem. Soc. Ethiop. **22**, 277 (2008).
33. M. Damnjanovic, I. Milosevic, T. Vukovic, and R. Sredanovic, Phys. Rev. B **60**, 2728 (1999).
34. M. Damnjanovic, T. Vukovic, and I. Milosevic, J. Phys. A: Math. Gen. **33**, 6561 (2000).
35. O. E. Alon, Phys. Rev. B **63**, 201403R (2001).
36. O. E. Alon, J. Phys.: Condens. Matter. **15**, 2489 (2003).
37. M. S. Dresselhaus, G. Dresselhaus, and A. Jorio, *Applications of Group Theory to the Physics of Condensed Matter* (Springer, New York, 2006).
38. M. Damnjanovic, I. Milosevic, T. Vukovic, and R. Sredanovic, Phys. Rev. B **60**, 2728 (1999).
39. M. Damnjanovic, Phys. Lett. A **94**, 337 (1983).
40. *Analytical Applications of Raman Spectroscopy,* Ed. by M. J. Pelletier (Kaiser Opt. Syst., Ann Arbor, MI, 1999).
41. R. Satio, T. Takeya, T. Kimura, et al., Phys. Rev. B **57**, 4145 (1998).
42. *HyperChem 7.0* (Hypecube Inc., Gainesville, FL, USA, 2001).
43. E. B. Wilson, Jr., J. C. Decius, and P. C. Cross, *Molecular Vibrations; The Theory of Infrared and Raman Vibrational Spectra* (McGraw-Hill, New York, 1955).
44. F. Albert, *Chemical Application of Group Theory* (Wiley-Intersci., New York, 1971).
45. L. Schafer and S. J. Cyvrin, J. Chem. Ed. **48**, 295 (1971).
46. D. P. Strommen and E. P. Lippincott, J. Chem. Ed. **48**, 295 (1971).
47. H. P. Fritzer, Match. **3**, 21 (1977).
48. J. M. Alvarino, J. Chem. Ed. **55**, 307 (1978).
49. R. L. Flurry, Jr., J. Chem. Ed. **55**, 638 (1979).
50. D. P. Strommen, J. Chem. Ed. **56**, 640 (1979).
51. J. M. Alvarino and A. Chammoro, J. Chem. Ed. **57**, 785 (1980).